EPR OF Gd^{3+}-DOPED $La_{0.9}Nd_{0.1}F_3$ CRYSTAL: SPIN–PHONON INTERACTIONS AND SPIN–LATTICE RELAXATIONS

M.L. PARADOWSKI* AND L.E. MISIAK

Institute of Physics, Maria Curie-Skłodowska University
Pl. M. Curie-Skłodowskiej 1, 20-031 Lublin, Poland

(Received June 5, 1998; revised version January 25, 1999)

The X-band EPR study of Gd^{3+}-doped $La_{0.9}Nd_{0.1}F_3$ single crystal in the temperature range 4.2–295 K is carried out in order to investigate crystal field effects, the Gd^{3+} spin–phonon interactions, as well as Gd^{3+} and Nd^{3+} spin–lattice relaxation times. The local distortions at 4.2 K of the positions of the eight F^- ions surrounding the Gd^{3+} ion in the $La_{0.9}Nd_{0.1}F_3$ crystal were determined from comparison of the theoretical with the experimental spin-Hamiltonian parameters. The spin–phonon interactions can be described by the Einstein model, which better characterizes the behavior of paramagnetic centers in LaF_3 and $La_{0.9}Nd_{0.1}F_3$ crystals than the Debye model. It is suggested, from the rotational invariance mechanism for phonon-induced contributions to spin-Hamiltonian parameters, that the rotational contributions are much smaller than those from the strain.

PACS numbers: 76.30.Kg

1. Introduction

The REF_3 (RE = Ce, Nd) crystals are expected to serve as heavy, fast, and radiation hard scintillators for calorimetry at future colliders [1, 2]. These crystals are also used as laser materials [3, 4].

The electron paramagnetic resonance (EPR) measurements of Gd^{3+}-doped LaF_3 and NdF_3 single crystals in the temperature range 4.2–295 K were previously performed by Misra et al. [5, 6]. The EPR linewidths were measured in Gd^{3+}-doped $La_xNd_{1-x}F_3$ ($0 \leq x \leq 1$) single crystals in the temperature range from 77 to 510 K [7, 8], whereas the magnetic susceptibility in the temperature range 1.5–300 K [9]. A temperature EPR (X-band) study of Gd^{3+}-doped (0.1 mol%) $La_{0.9}Nd_{0.1}F_3$ single crystal has been carried out presently in order to

*e-mail: mlpar@tytan.umcs.lublin.pl

investigate structural and crystal field effects, spin–phonon interactions, and dipolar interactions between Gd^{3+} and Nd^{3+} ions. The above sample is the only mixed crystal studied in detail for which well-resolved EPR spectra can be recorded down to liquid-helium temperature.

2. Sample preparation and crystal structure

The $La_xNd_{1-x}F_3$ single crystals doped with Gd^{3+} (0.1 mol%) were grown by a modified Bridgman–Stockbarger method [10]. They were transparent and cleft easily in the cleavage planes (001) and (110).

LaF_3 and NdF_3 single crystals have a tysonite structure with the trigonal space-group classification $P\bar{3}c1$ (D^4_{3d} trigonal symmetry with a hexamolecular unit cell) [11, 12]. The site symmetry of the La^{3+} and the Nd^{3+} ions is C_2. The twofold axis is perpendicular to the threefold axis C_3 in the unit cell. The crystallographic a axis forms an angle of 30° with respect to one of the three C_2 axes, where the two remaining C_2 axes form an angle of 90° and 150° with respect to a axis, respectively. The crystallographic c axis is parallel to the C_3 axis, and perpendicular to the three C_2 axes. There are six molecules per unit cell. The unit cell parameters for LaF_3 are as follows: $a = 0.7186 \pm 0.0001$ nm, $c = 0.7352 \pm 0.0001$ nm, while for NdF_3 are: $a = 0.7032 \pm 0.0001$ nm and $c = 0.7200 \pm 0.0001$ nm at room temperature [10]. Since the values of a and c and the distances of the rare-earth in LaF_3 and NdF_3 are quite close to each other, it is assumed that $La_xNd_{1-x}F_3$ single crystals also have a tysonite structure, with the a and c dimensions scaled in proportion to x between limit values of lattice constants in LaF_3 and NdF_3 [13].

3. Experimental details

The experimental arrangement has been described elsewhere [14]. The EPR spectra of the Gd^{3+} ions in $La_{0.9}Nd_{0.1}F_3$ single crystal were recorded with the external magnetic field $\boldsymbol{B}$ oriented in the ZX plane. The $\boldsymbol{Z}$ ($\parallel a$) axis, along which the overall splitting of EPR lines has a maximum, lies in the cleavage plane (001) and is perpendicular to the (110) plane. The X axis is defined to be the direction of the external magnetic field for which the next-largest extremum occurs. The $\boldsymbol{Y}$ ($\parallel c$) axis is defined to be the direction for which the minimum splitting of EPR lines is observed.

The angular variation for Gd^{3+}-doped $La_{0.9}Nd_{0.1}F_3$ in the ZX plane at 295 K is shown in Fig. 1. These variations in the ZX plane at room and liquid nitrogen temperatures were found to display three maxima and minima of the three centers placed by 60° from each other. The six ions in the unit cell were found to be magnetically equivalent in pairs, so that there are three magnetically nonequivalent sites of Gd^{3+} ions forming three observed centers [15]. Thus, EPR spectra are consistent with the rhombic C_{2v} site symmetry for the Gd^{3+} ion in the D^4_{3d} trigonal symmetry with a hexamolecular unit cell. However, only two centers were observed at liquid helium temperature: the $Gd^{3+}(1)$ center which exhibits the twofold repetition pattern about the c axis (Y axis) and the $Gd^{3+}(2)$ center exhibiting the site symmetry close to monoclinic C_2. It means that the crystal field is changed with lowering the temperature, as a result of the temperature-induced distortion of the crystal lattice [15].

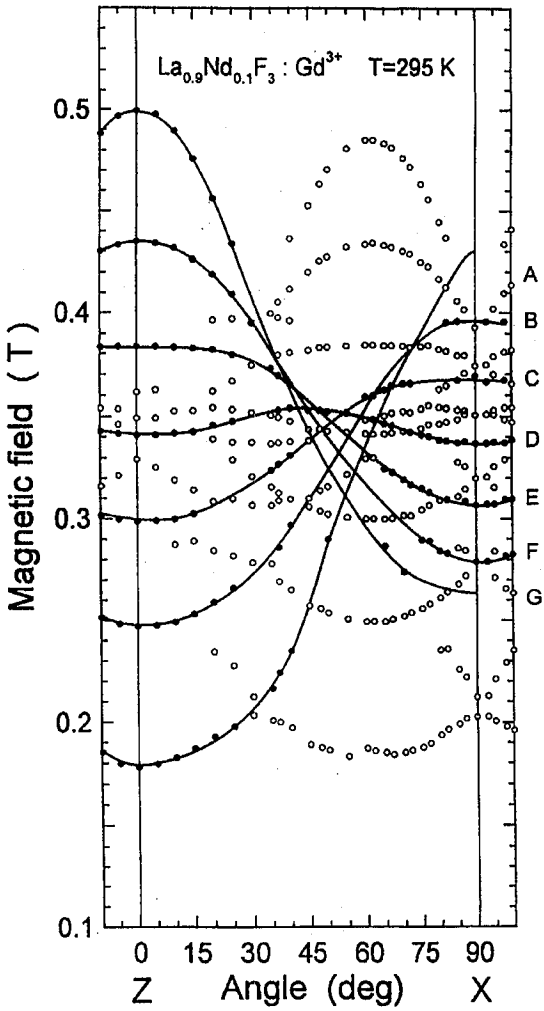

Fig. 1. Angular variation of the EPR lines positions in the ZX plane for Gd^{3+}-doped $La_{0.9}Nd_{0.1}F_3$ single crystal at room temperature. The dots represent the experimental resonant line positions of $\Delta M = \pm 1$ transitions and the solid lines (as a guide for the eye) are smooth curves that connect data points from the same transitions, corresponding to one set (called $Gd^{3+}(1)$ center) of magnetically equivalent ions. The circles, which represent the experimental line positions of the $Gd^{3+}(2)$ center, are not connected. The transitions are indicated as follows: $A(\frac{7}{2} \leftrightarrow \frac{5}{2})$, $B(\frac{5}{2} \leftrightarrow \frac{3}{2})$, $C(\frac{3}{2} \leftrightarrow \frac{1}{2})$, $D(\frac{1}{2} \leftrightarrow -\frac{1}{2})$, $E(-\frac{1}{2} \leftrightarrow -\frac{3}{2})$, $F(-\frac{3}{2} \leftrightarrow -\frac{5}{2})$, $G(-\frac{5}{2} \leftrightarrow -\frac{7}{2})$.

The average linewidths (peak-to-peak of the first derivative lineshape) ΔB_{pp} of the seven EPR lines characterizing the rhombic C_{2v} site symmetry of Gd^{3+} in $La_{0.9}Nd_{0.1}F_3$ (for $\boldsymbol{B} \parallel \boldsymbol{Z}$) are equal to 13.8 ± 0.8 mT, 10.8 ± 0.8 mT, 9.4 ± 0.6 mT, 8.5 ± 0.6 mT, and 8.1 ± 0.6 mT at 4.2, 22, 50, 77, and 295 K, respectively. In LaF_3 average ΔB_{pp} are about 2.5 ± 0.3 mT in the temperature range 4.2–295 K [5].

4. Spin-Hamiltonian parameters (SHP) and superposition model calculations

The spin Hamiltonian describing Gd^{3+} ion in the rhombic C_{2v} symmetry of the crystal field is given as

$$\mathcal{H} = \tilde{g}\mu_B \boldsymbol{BS} + \sum_{m=0,2} \frac{1}{3} b_2^m O_2^m + \sum_{m=0,2,4} \frac{1}{60} b_4^m O_4^m + \sum_{m=0,2,4,6} \frac{1}{1260} b_6^m O_6^m. \quad (1)$$

The symbols have their usual meaning as defined by Abragam and Bleaney [16]. The S ($= \frac{7}{2}$) is the electron spin of the Gd^{3+} ion. The eleven SHP's for Gd^{3+} in $La_{0.9}Nd_{0.1}F_3$ single crystal were evaluated using a least-squares fitting procedure [17] for fitting simultaneously all resonant line positions recorded in the ZX plane (Table I).

TABLE I

Values of the spin-Hamiltonian parameters in Gd^{3+}-doped $La_{0.9}Nd_{0.1}F_3$ single crystal at various temperatures. The b_l^m parameters are expressed in GHz, while g_{zz} and g_{xx} are dimensionless; n represents the total number of line positions simultaneously fitted. SMD [GHz^2] $= \sum_j (|\Delta E_j| - h\nu_j)^2$, where ΔE_j is the calculated energy difference between levels participating in resonance for the j-th resonance magnetic field, and $h\nu_j$ is the microwave energy. The coefficient α represents the admixture of state $^6P_{7/2}$ in the state $^8S_{7/2}$.

T [K]	295	77	50	22	4.2
g_{zz}	1.993 ± 0.002	1.983 ± 0.003	1.998 ± 0.013	1.991 ± 0.013	1.963 ± 0.013
g_{xx}	1.990 ± 0.002	1.988 ± 0.004	1.971 ± 0.012	1.981 ± 0.012	1.999 ± 0.012
b_2^0	0.696 ± 0.003	0.698 ± 0.003	0.674 ± 0.011	0.647 ± 0.009	0.652 ± 0.005
b_2^2	-0.121 ± 0.009	-0.045 ± 0.014	-0.155 ± 0.032	-0.167 ± 0.028	-0.140 ± 0.021
b_4^0	0.017 ± 0.001	0.017 ± 0.001	0.021 ± 0.004	0.014 ± 0.003	0.022 ± 0.001
b_4^2	0.045 ± 0.007	0.027 ± 0.009	0.024 ± 0.015	0.018 ± 0.012	0.013 ± 0.012
b_4^4	0.035 ± 0.011	0.065 ± 0.015	0.070 ± 0.031	0.072 ± 0.025	0.119 ± 0.019
b_6^0	-0.001 ± 0.001	-0.001 ± 0.001	0.003 ± 0.005	-0.000 ± 0.003	-0.006 ± 0.002
b_6^2	0.010 ± 0.011	0.004 ± 0.013	0.126 ± 0.082	-0.049 ± 0.032	0.006 ± 0.018
b_6^4	-0.030 ± 0.018	-0.056 ± 0.022	-0.080 ± 0.022	-0.279 ± 0.029	0.064 ± 0.029
b_6^6	-0.028 ± 0.019	-0.009 ± 0.032	-0.279 ± 0.109	-0.051 ± 0.041	-0.101 ± 0.039
n	125	94	12	34	65
SMD	0.208	0.151	0.098	0.127	0.684
α	0.19 ± 0.02	0.24 ± 0.02	0.25 ± 0.09	0.24 ± 0.06	0.27 ± 0.03

The crystal-field parameters b_l^m and the zero-field splittings ΔE of Gd^{3+} in LaF_3 and $La_{0.9}Nd_{0.1}F_3$ hosts can be fitted in the temperature range 4.2–295 K to the quadratic function, $a + bT + cT^2$, where the values of a, b, c are included in Table II. A quadratic temperature dependence of b_l^m was observed for Gd^{3+} in $LiY_{1-x}Yb_xF_4$ hosts [14, 18], assuming the temperature dependence is due to static distortion. On the other hand, vibrational effects of the crystal lattice cause temperature dependence of b_l^m which can be fitted to the equation containing terms $\sum_i d_i \coth\left(\frac{h\nu_i}{2kT}\right)$, where ν_i are the lattice vibration frequencies and d_i are

TABLE II

Values of the constants required to fit the spin-Hamiltonian parameters and the zero-field splitting: (b_l^m and ΔE) $= a + bT + cT^2$ in the temperature range 4.2–295 K. The χ^2 values characterizing these fits are also included.

Sample		a [GHz]	b [GHz · K^{-1}]	c [GHz · K^{-2}]	χ^2 [GHz^2]
LaF_3	b_2^0	0.7015	0.6310×10^{-5}	-0.1042×10^{-6}	5.2362×10^{-5}
	b_2^2	-0.1110×10^{-1}	-0.5737×10^{-3}	0.1132×10^{-5}	2.2955×10^{-4}
	b_4^0	0.1885×10^{-1}	-0.6496×10^{-4}	0.1902×10^{-6}	2.6879×10^{-6}
	b_4^2	0.5383×10^{-1}	0.1284×10^{-3}	-0.3059×10^{-6}	1.5557×10^{-4}
	b_4^4	0.1212	-0.3751×10^{-3}	0.1211×10^{-5}	9.0903×10^{-6}
	ΔE	8.3503	0.1286×10^{-2}	-0.3955×10^{-5}	3.2892×10^{-3}
$La_{0.9}Nd_{0.1}F_3$	b_2^0	0.6412	0.8183×10^{-3}	-0.2146×10^{-5}	2.2482×10^{-4}
	b_2^2	−0.1750	0.1516×10^{-2}	-0.4508×10^{-5}	4.9005×10^{-3}
	b_4^0	0.1894×10^{-1}	-0.8995×10^{-5}	7.6012×10^{-8}	4.1983×10^{-5}
	b_4^2	0.1434×10^{-1}	0.1713×10^{-3}	-0.2285×10^{-6}	8.5805×10^{-6}
	b_4^4	0.1063	-0.7255×10^{-3}	0.1658×10^{-5}	6.3936×10^{-4}
	ΔE	7.8387	0.8402×10^{-2}	-0.2156×10^{-4}	5.9427×10^{-3}

the weighting parameters [19]. These terms in temperature expansion of $b_l^m(T)$ will then contain terms in T, T^2, and higher powers.

The SHP's for Gd^{3+}-doped $La_{0.9}Nd_{0.1}F_3$ single crystal can be analyzed using the superposition model [20]. In this model the b_l^m are expressed as linear superpositions of single-ligand contributions to the intrinsic parameters $\bar{b}_l(R_0)$ which depend on the ligand i as follows:

$$b_l^m = \sum_i \bar{b}_l(R_i) K_l^m(\theta_i, \varphi_i), \tag{2}$$

where

$$\bar{b}_l(R_i) = \bar{b}_l(R_0)(R_0/R_i)^{t_l}. \tag{3}$$

The R_i's in Eqs. (2) and (3) are the distances of the ligand F^- ions from the Gd^{3+} ion, θ_i is the polar angle of the i-th F^- ion with respect to the Z axis, φ_i is the azimuthal angle of the i-th F^- ion with respect to the X axis and the R_0 is a particular bond length, used as a reference (i.e. the minimum distance $F^- - Gd^{3+}$). The K_l^m in Eq. (2) are angular functions related to the spherical harmonics [21].

For the $La_xNd_{1-x}F_3$ single crystals ($x = 1$, 0.9, 0.1), we consider the nine nearest neighbor F^- ions to a Gd^{3+} ion which substitute for La^{3+}, or Nd^{3+} ion (Fig. 2). The required positions (R_i, θ_i, φ_i) for LaF_3 and NdF_3 are given in Ref. [6]. In order to evaluate the intrinsic parameters $\bar{b}_l(R_0)$, the required lattice constants of $La_{0.9}Nd_{0.1}F_3$ were estimated using Vegard's law [13]. The unit cell parameters of LaF_3 and NdF_3 were measured in the range 87–295 K [10]; those parameters at lower temperatures were obtained by extrapolation. The application of the superposition model requires exact knowledge of t_l intrinsic exponential parameters and positions of ligands around the paramagnetic ion. In our case we assumed that $t_2 = 9$ and $t_4 = 14$, which are the same as those for LaF_3 and NdF_3 hosts [6]. The angular coordinations of F^- ligands were changed independently in the calculations from Ref. [6]. We propose to change the angles

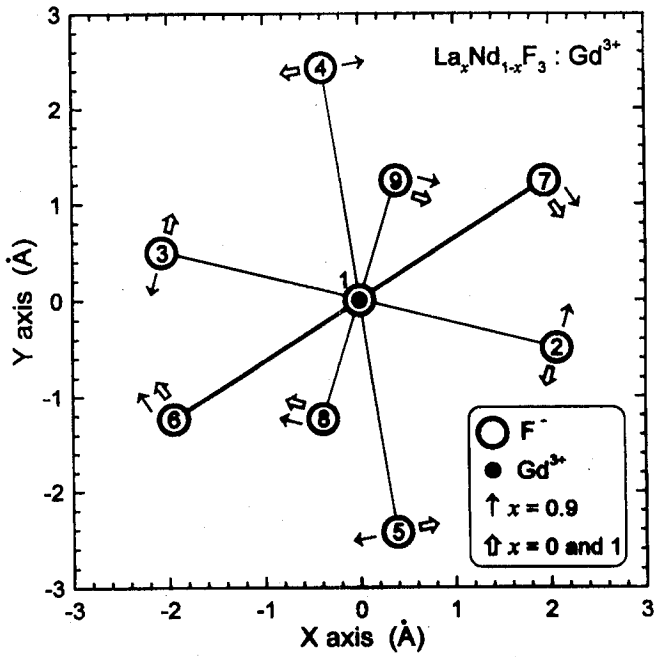

Fig. 2. The projection of F^- ions onto the XY plane showing the deformation of the $La_xNd_{1-x}F_3$ host lattice at room temperature after the Gd^{3+} ion substitute for the La^{3+} or the Nd^{3+} ion. The fluorine ion 1 is above the plane and sets the Z axis. The fluorine ions 6 and 7 lie above the XY plane (connection to the Gd^{3+} ion marked by solid thick lines), whereas remaining fluorides lie below this plane (thin lines).

φ of F^- pairs at the coordinates (R, θ, φ) and $(R, \theta, \varphi + 180°)$ by the same values. In our calculations for Gd^{3+}-doped LaF_3, $La_{0.9}Nd_{0.1}F_3$ and NdF_3 we have attempted a direct fitting to the experimental parameters b_l^m, allowing the angular azimuthal coordinates for eight F^- ligands (grouped in pairs) to vary within $\Delta\varphi = \pm 3.5°$ ($\Delta\varphi = \varphi_{\text{final}} - \varphi_{\text{initial}}$). The deformation (rotation) is around the Z-axis; i.e. the F^- ions rotate in the XY plane perpendicular to the crystallographic a axis, according to arrows in Fig. 2. Combining Eqs. (2) with (3) we were able to compute angles of local distortions ($\Delta\varphi$) of eight ligands grouped in pairs, intrinsic parameters $\overline{b}_2$ and $\overline{b}_4$, and theoretical values of b_l^m at various temperatures (Table III). There is a good agreement of the calculated theoretical value with the experimental values of the b_l^m, supporting the above mechanism of distortion. There are local distortions (rotations) in opposite directions $\Delta\varphi$ for 2–3 and 4–5 F^- pairs in $La_{0.9}Nd_{0.1}F_3$ (Fig. 2), contrary to those in LaF_3 and NdF_3 at room temperature, where only 4–5 F^- pairs are rotated in direction opposite to other F^- pairs. The rotation changes to opposite directions for 4–5 and 8–9 F^- pairs are also observed in $La_{0.9}Nd_{0.1}F_3$ when temperature is lowering down to 4.2 K (see Table III). This confirms our earlier suggestion [15] that the crystal field in $La_{0.9}Nd_{0.1}F_3$ is changed with lowering temperature, as a result of temperature

TABLE III

The experimental (Exp.) and theoretical calculated from superposition model (Theo.) values of spin-Hamiltonian parameters b_l^m (in GHz). The intrinsic parameters $\bar{b}_l$ (in GHz) and the local distortion measured by azimuthal angles $\Delta\varphi_{i,j}$ (in degrees) from Gd^{3+} ion to eight surrounding F^- ions are also included; R_0 is the minimum distance between $Gd^{3+} - F^-$ ions. $\Delta E = E(\pm\frac{7}{2}) - E(\pm\frac{1}{2})$ (in GHz) is the zero-field splitting.

Sample	LaF_3		$La_{0.9}Nd_{0.1}F_3$										NdF_3	
T [K]	295		295		77		50		22		4.2		295	
	Exp.[a]	Theo.	Exp.	Theo.	Exp.	Theo.	Exp.	Theo.	Exp.	Theo.	Exp.	Theo.	Exp.[a]	Theo.
b_2^0	0.694	0.707	0.696	0.691	0.698	0.697	0.674	0.677	0.647	0.648	0.652	0.654	0.802	0.809
b_2^2	−0.083	−0.082	−0.121	−0.122	−0.045	−0.045	−0.155	−0.154	−0.167	−0.167	−0.140	−0.140	−0.148	−0.147
b_4^0	0.016	0.016	0.017	0.014	0.017	0.014	0.021	0.016	0.014	0.011	0.022	0.016	0.019	0.019
b_4^2	0.066	0.072	0.045	0.053	0.027	0.057	0.024	0.064	0.018	0.046	0.013	0.071	0.081	0.084
b_4^4	0.117	0.108	0.035	0.038	0.065	0.052	0.070	0.053	0.072	0.056	0.119	0.084	0.130	0.127
$\bar{b}_2$	-4.616 ± 0.050		-4.547 ± 0.046		-4.622 ± 0.080		-4.470 ± 0.096		-4.250 ± 0.089		-4.273 ± 0.081		-5.497 ± 0.050	
$\bar{b}_4$	0.018 ± 0.001		0.015 ± 0.003		0.015 ± 0.002		0.018 ± 0.008		0.012 ± 0.005		0.018 ± 0.002		0.021 ± 0.001	
$\Delta\varphi_{2,3}$	2.0 ± 0.5		-3.5 ± 0.5		-3.5 ± 0.5		-3.5 ± 0.5		0.0 ± 0.5		-3.5 ± 0.5		2.0 ± 0.5	
$\Delta\varphi_{4,5}$	-3.5 ± 0.5		3.5 ± 0.5		1.0 ± 0.5		2.5 ± 0.5		0.0 ± 0.5		-3.0 ± 0.5		-3.5 ± 0.5	
$\Delta\varphi_{6,7}$	3.5 ± 0.5		3.0 ± 0.5		2.5 ± 0.5		2.5 ± 0.5		3.5 ± 0.5		1.0 ± 0.5		3.5 ± 0.5	
$\Delta\varphi_{8,9}$	2.0 ± 0.5		3.0 ± 0.5		-1.0 ± 0.5		2.0 ± 0.5		0.5 ± 0.5		-3.5 ± 0.5		3.0 ± 0.5	
R_0 [Å]	2.4187		2.4133		2.4089		2.4090		2.4092		2.4093		2.3663	
ΔE	8.39 ± 0.10[a]		8.44 ± 0.04		8.36 ± 0.05		8.23 ± 0.20		7.95 ± 0.15		7.91 ± 0.08		9.80 ± 0.10[a]	

[a]The experimental SHP's were taken from Refs. [6] and P. Mikołajczak, Hab. Thesis, Maria Curie-Skłodowska University, Lublin 1982.

induced distortion of crystal lattice which causes the change of the site symmetry of Gd^{3+} ion from C_{2v} at 77 K towards close C_2 at 4.2 K. In LaF_3 any rotation changes to opposite directions are not observed with lowering temperature down to 4.2 K. The distortions of four fluorine pairs in the same directions as at 295 K only remain.

5. Debye and Einstein models of phonon spectrum

The major part of the temperature dependence of b_2^0 is due to the spin–phonon interaction effects [14]. The b_2^0 parameter changes its value as much as $\Delta b_2^0 = 0.0073$ GHz (100%) in the temperature range 87–295 K for LaF_3. Using the data of lattice constants dependent on temperature [10] and the equation for $\bar{b}_2$ obtained from Eqs. (2), (3) we evaluate to 0.0024 GHz (about 33%) the contribution of thermal expansion to Δb_2^0. The remaining part (67%) of the b_2^0 change with temperature is due to the modulation of the crystal field by thermally excited phonons. Thus, the temperature dependence of the b_2^0 can be ascribed to the spin–phonon interaction. The Debye model in the long-wavelength limit gives [22, 23]:

$$b_2^0(T) = b_2^0(0)\left(1 - C\frac{T^4}{\theta_D^4}\int_0^{\theta_D/T}\frac{x^3}{e^x - 1}dx\right), \tag{4}$$

where C is a constant and θ_D is the Debye temperature. On the other hand, the Einstein model involving a single oscillator gives

$$b_2^0(T) = b_2^0(0)\left\{1 - C\left[\coth\left(\frac{h\nu}{2kT}\right) - 1\right]\right\}, \tag{5}$$

where $h\nu$ is energy of the interacting phonon mode. The parameters for the best fit of the b_2^0 to temperature in $La_{0.9}Nd_{0.1}F_3$ (LaF_3) for the Debye model are

$b_2^0(0) = 0.653 \pm 0.063$ GHz (0.703 ± 0.070 GHz),

$C = 0.110 \pm 0.011$ (-0.003 ± 0.005),

$\theta_D' = 224 \pm 12$ K (218 ± 8 K),

$\chi^2 = 1.05 \times 10^{-4}$ GHz^2 (1.75×10^{-4} GHz^2).

On the other hand, the parameters providing the best fit using the Einstein model are

$b_2^0(0) = 0.668 \pm 0.067$ GHz (0.704 ± 0.052 GHz),

$C = -0.071 \pm 0.008$ (0.022 ± 0.008),

$h\nu/k = 434 \pm 16$ K (406 ± 15 K),

$\chi^2 = 1.58 \times 10^{-3}$ GHz^2 (1.01×10^{-4} GHz^2).

There is a good agreement between the $b_2^0(0)$ values of both models for $La_{0.9}Nd_{0.1}F_3$ and LaF_3 single crystals, confirming the correctness of the fitting. The effective Debye temperatures θ_D' for $La_{0.9}Nd_{0.1}F_3$ and LaF_3, equal to 224 K and 218 K, respectively, seem to be too low and it is concluded that the errors originate in the use of the Debye model. The energies of single Einstein oscillators $h\nu/k$

used in Eq. (5) are equal to 434 K and 406 K for $La_{0.9}Nd_{0.1}F_3(Gd^{3+})$ and LaF_3 (Gd^{3+}) respectively, and their values are more close to those 382 K and 387 K reported for LaF_3 and NdF_3 in Ref. [24]. The ratio of θ'_D to $h\nu/k$ is equal to 0.5 for both samples and means that the Einstein model yields an interaction with somewhat higher-frequency phonons than the Debye model. The ratio is different from that equal to 1.4 determined in $LiYF_4$ [25] and $BaTiO_3$ [23]. It is clear that in $La_xNd_{1-x}F_3(Gd^{3+})$ system are produced higher frequency phonon modes than in $LiYF_4(Gd^{3+})$ and $BaTiO_3(Cr^{3+})$, presumably due to higher difference of masses of composite ions, as well as to more simple system than in case of $LiYF_4$ and $BaTiO_3$. It is concluded that average phonon spectrum shifts to somewhat shorter wavelength values in $La_xNd_{1-x}F_3(Gd^{3+})$ ($x = 1$, 0.9) than long-wavelength limit described by the Debye model (Eq. (4)). The Einstein model of single oscillator better describes the paramagnetic center behavior, i.e., the temperature dependence of b_2^0 parameter, particularly in the case of the presence of one kind of paramagnetic ions (for Gd^{3+}-doped LaF_3 crystal). Further, the average energy of thermally excited optical phonons is presently determined to be 282 cm^{-1} for Gd^{3+}-doped LaF_3 and 302 cm^{-1} for Gd^{3+}-doped $La_{0.9}Nd_{0.1}F_3$. The optical phonons of E_g symmetry were observed at 293, 299.8 and 315.1 cm^{-1} in LaF_3 [26]. The Stokes vibronic emission lines in Gd^{3+}-doped LaF_3 at 4.2 K are reported to be 179, 289, 318, 362, and 433 cm^{-1} [27]. Further, in Raman spectra of LaF_3 and NdF_3 were observed strong "phonon E_g type" bands at 290 cm^{-1} in LaF_3, and at 314 cm^{-1} in NdF_3 [28]. Taking into account the above comparison, our estimation of optical phonons energy from EPR data is in sufficiently good agreement with those given in the literature.

The average velocity of sound v_m can be estimated from the relation [29]:

$$v_m = \frac{\theta_D}{\frac{h}{k}\left(\frac{3q}{4\pi}\frac{N\rho}{M}\right)^{1/3}}, \tag{6}$$

where ρ is the density of LaF_3 (5.94 g cm^{-3}) or $La_{0.9}Nd_{0.1}F_3$ (6.16 g cm^{-3}), q is the number of atoms in the molecule (4 in these crystals), N is the Avogadro number and M is the molar mass.

The calculated velocities of sound v_m from Eq. (6), using θ_D ($= h\nu/k$) equal to 406 K for LaF_3 and to 434 K for $La_{0.9}Nd_{0.1}F_3$, are 3.26×10^5 cm s^{-1} and 3.45×10^5 cm s^{-1}, respectively. The velocity of sound in the XY plane of LaF_3 at room temperature was calculated in Ref. [24] as equal to 2.78×10^5 cm s^{-1}. Schulz and Jeffries [30] measured the velocity of sound in LaF_3 single crystal and received in average 3.44×10^5 cm s^{-1}. Our calculated v_m's are quite close to that of measured by Schulz and Jeffries [30] supporting the value of $\theta_D = 406$ K in LaF_3 to be more realistic than 382 K calculated in Ref. [24].

Below we consider the successful use of intrinsic parameters to describe the spin–phonon interactions in rare-earth trifluorides. The temperature dependence of b_2^0 value is reflected by the change in the value of the intrinsic parameter $\bar{b}_2$ with temperature, because the effect of thermal expansion (contraction) of the lattice on $\bar{b}_2$ is calculated to be rather small. In order to describe the temperature dependence of $\bar{b}_2$ we used the transformed isotropic Einstein model for lattice

vibration [31], which contains the coupling between Gd^{3+} spin and one localized mode

$$\bar{b}_2(T) = \bar{b}_2(\mathrm{RL}) + K_2 \coth\left(\frac{h\nu}{2kT}\right), \tag{7}$$

where $\bar{b}_2(\mathrm{RL})$ is a "rigid lattice" value of $\bar{b}_2$ (i.e. the value of $\bar{b}_2$ at $T = 0$ K minus zero point vibrations) and K_2 is the coupling constant describing the magnitude of Gd^{3+} spin–phonon interaction. The $\bar{b}_2(\mathrm{RL})$, K_2 estimated from the fitting to Eq. (7) yield values -4.75 ± 0.05, 0.13 ± 0.02 GHz for $La_{0.9}Nd_{0.1}F_3$ and -4.85 ± 0.05, 0.14 ± 0.02 GHz for LaF_3, respectively.

On the other hand, the Debye model assumes that paramagnetic ions (Gd^{3+}) are coupled to the whole phonon spectrum of the crystal lattice. The equation adopted to fit $\bar{b}_2$ to temperature is the following [32]:

$$\bar{b}_2(T) = \bar{b}_2(\mathrm{RL}) + K_2\left(1 + 8\frac{T^4}{\theta_\mathrm{D}^4}\int_0^{\theta_\mathrm{D}/T}\frac{x^3}{\mathrm{e}^x - 1}\mathrm{d}x\right). \tag{8}$$

The best fit with $\theta_\mathrm{D} = 434$ K and 406 K for $La_{0.9}Nd_{0.1}F_3$ and LaF_3, respectively, yields the following parameters:

$$\bar{b}_2(\mathrm{RL}) = -4.71 \pm 0.06 \text{ GHz}, \qquad K_2 = 0.08 \pm 0.04 \text{ GHz } (La_{0.9}Nd_{0.1}F_3)$$

and

$$\bar{b}_2(\mathrm{RL}) = -4.81 \pm 0.05 \text{ GHz}, \qquad K_2 = 0.09 \pm 0.03 \text{ GHz } (LaF_3).$$

The above $\bar{b}_2$ (RL) and K_2 values derived from the Einstein and the Debye models are equal to each other within errors, confirming the correctness of the fitting.

The coupling between spins and phonons (K_2) in LaF_3 (Gd^{3+}) is about four times greater than in $LiYF_4$ (Gd^{3+}) crystal [18]. This statement can be confirmed by optical measurements [33], implying a larger amplitude of zero vibrations of the lattice in LaF_3 (4.69×10^{-3} nm) versus $LiYF_4$ (3.77×10^{-3} nm).

6. Rotational invariance and the phonon-induced contributions to SHP

The theory of rotational invariance for the phonon-induced contributions to spin-Hamiltonian parameters developed by Bates and Szymczak [34, 35] gives more precise description of the observed contribution to the b_2^0 from lattice dynamics. It is usually difficult to determine magnetoelastic tensor components in low symmetry crystal field, e.g., in REF_3 crystals. In order to explain experimentally measured SHP's by the above mechanism we need to separate the thermal expansion from that of the spin–phonon contributions. In order to separate the spin–phonon contribution we used the $\bar{b}_2$ values determined from superposition model as follows: $\delta\mathcal{D} \approx 0.67 \cdot \delta\bar{b}_2 = 0.67[\bar{b}_2(295) - \bar{b}_2(\mathrm{RL})]$. (In Sec. 5 we evaluated to 67% the spin–phonon contribution, the rest part is the contribution from thermal expansion.) Thus, these spin–phonon contributions ($\delta\mathcal{D}$) are equal to 0.106 ± 0.036 GHz and 0.129 ± 0.034 GHz for Gd^{3+}-doped $La_{0.9}Nd_{0.1}F_3$ and LaF_3, respectively.

Further, the anharmonic contributions $\delta\mathcal{D}$ and $\delta\mathcal{D}_\mathrm{r}$ to $\mathcal{D}$ are given by the equations [35]:

$$\delta\mathcal{D} = \frac{-\hbar}{32\pi^2\rho}(G_{11} + G_{12} + G_{13})(v_\mathrm{l}^{-5} + 2v_\mathrm{t}^{-5})f(\omega_\mathrm{D}, T), \tag{9}$$

and

$$\delta\mathcal{D}_r = \frac{-\hbar}{32\pi^2\rho}\mathcal{D}v_t^{-5}f(\omega_D, T), \tag{10}$$

where G_{11}, G_{12}, G_{13} are the components of the magnetoelastic tensor, v_l and v_t are longitudinal and transversal velocities of sound, respectively, and

$$f(\omega_D, T) = \omega_D^4 + 8\left(\frac{kT}{\hbar}\right)^4 \int_0^{\theta_D/T} \frac{x^3}{e^x - 1}dx \tag{11}$$

with $\hbar\omega_D = k\theta_D$.

The values of sound velocities are $v_l = 6.02 \times 10^5$ cm s^{-1}, $v_t = 2.31 \times 10^5$ cm s^{-1} for $La_{0.9}Nd_{0.1}F_3$ and $v_l = 5.69 \times 10^5$ cm s^{-1}, $v_t = 2.18 \times 10^5$ cm s^{-1} for LaF_3.

The calculation yields the sum values of magnetoelastic tensor components $(G_{11} + G_{12} + G_{13})$ to be -3.04 ± 1.00 and -3.33 ± 0.88 GHz for $La_{0.9}Nd_{0.1}F_3$ and LaF_3, respectively. Further, from Eq. (10) $\delta\mathcal{D}_r$ was determined to be -0.0121 ± 0.0014 and -0.0134 ± 0.0017 GHz, as well as the ratio $\mathcal{R}_D$ $(= \delta\mathcal{D}_r/\delta\mathcal{D})$ to be -0.11 and -0.10 for $La_{0.9}Nd_{0.1}F_3$ and LaF_3, respectively. This result is in agreement with those obtained in [35] using the isotropic continuum phonon model for orbital singlet ions in low symmetry crystal field; i.e. the rotational contributions are much smaller than those from the strain. In addition, we determined that the spin–phonon interaction constant K_2 given by Eq. (8) could be expressed in terms of the magnetoelastic tensor components as follows:

$$K_2 = \frac{-\hbar\omega_D^4\left(v_l^{-5} + 2v_t^{-5}\right)}{21.44\pi^2\rho}(G_{11} + G_{12} + G_{13}). \tag{12}$$

7. Nd^{3+} and Gd^{3+} spin–lattice relaxation times

The full linewidth at half peak of a Gaussian distribution due to dipole–dipole and exchange interactions, is given by the expression [36, 37]:

$$\Delta B_{dip-ex}^2 = \frac{(2.35)^2h^2\langle\Delta\nu^2\rangle_{av}}{g^2\mu_B^2}. \tag{13}$$

The dipolar interactions between similar ions can be neglected because the distances between Gd^{3+} ions are sufficiently large in doped crystals. Taking into account dipolar and exchange interactions between dissimilar Gd^{3+} and Nd^{3+} ions the following expression is finally obtained for the second moment [38]:

$$\langle\Delta\nu^2\rangle_{av} = \frac{1}{3}S'(S'+1)h^{-2}$$

$$\times\left[zJ_p^2 + 2J_pG\sum_{k'}^{z}(1 - 3\gamma_{jk'}^2)r_{jk'}^{-3} + G^2\sum_{k'}^{z}(1 - 3\gamma_{jk'}^2)^2r_{jk'}^{-6}\right], \tag{14}$$

where $G = gg'\mu_B^2\mu_0$, h is the Planck constant, g and g' are Gd^{3+} and host Nd^{3+} g-factor, respectively, S' $(= \frac{1}{2})$ is the effective spin of Nd^{3+} host ion, μ_B is the Bohr magneton, $\mu_0 = 4\pi \times 10^{-7}$ H m^{-1}, J_p is the average host–impurity pair exchange constant, z $(= 1)$ is the number of paramagnetic neighbor Nd^{3+} ions

to a Gd^{3+} ion in $La_{0.9}Nd_{0.1}F_3$ (the remaining neighbors are La^{3+} ions), $r_{jk'}$ are the distances between the j and k' ions, and $\gamma_{jk'}$ are the direction cosines of $r_{jk'}$ with the magnetic field $\boldsymbol{B} \parallel \boldsymbol{Z}$. The Gd^{3+}–Nd^{3+} average pair exchange-interaction constant J_p ($\mathcal{H}_p = J_p \boldsymbol{S}\boldsymbol{S}'$) is estimated for the paramagnetic host $La_{0.9}Nd_{0.1}F_3$ to be $J_p = -2.7 \pm 0.5$ GHz [15]. The effective host g' value is determined from the Boltzmann weighting of the g_i value for each of the five Kramers doublets in the $^4I_{9/2}$ ground multiplet of Nd^{3+} ion in $La_{0.9}Nd_{0.1}F_3$ as follows [39]:

$$g' = \frac{\sum_{i=1}^{5} g_i \exp(-\Delta_i/kT)}{\sum_{i=1}^{5} \exp(-\Delta_i/kT)}, \tag{15}$$

where Δ_i is energy of the i-th doublet. The g_i values are taken from Ref. [9]. From Eq. (15), the effective g' values, along the Z-axis, have been determined to be 2.40, 2.87, and 3.39 at 4.2, 77, and 295 K, respectively.

The EPR linewidths $\Delta B_{pp}^{c} (= \Delta B_{dip-ex}/1.18)$ of Gd^{3+} in $La_{0.9}Nd_{0.1}F_3$ crystal for $\boldsymbol{B} \parallel \boldsymbol{Z}$ are calculated, from Eqs. (13) and (14), to be 370, 438, and 510 mT at 4.2, 77, and 295 K, respectively. The main contribution to these linewidths comes from dipole–dipole interactions whereas contribution from exchange interactions is not larger than 4%. The measured EPR linewidths ΔB_{pp} in this crystal equal to 13.8, 8.5, and 8.1 mT at 4.2, 77, and 295 K, respectively, are several times narrower than calculated ΔB_{pp}^{c}. This strong and temperature dependent narrowing of the EPR resonance lines can be explained with the mechanism of the spin–lattice modulated narrowing proposed by Mitsuma [40]. Finally, the spin–lattice relaxation time of the host Nd^{3+} ions can be determined from the expression

$$\tau_1' = \frac{3}{20} \frac{h \Delta B_{1/2}}{g' \mu_B \Delta B_{dip-ex}^2}. \tag{16}$$

The EPR lines of Gd^{3+}-doped $La_{0.9}Nd_{0.1}F_3$ (and LaF_3) crystals have a Lorentzian shape at all temperatures of investigation ($\Delta B_{1/2} = \sqrt{3} \Delta B_{pp}$). The superhyperfine interactions of Gd^{3+} ion with the neighboring ^{19}F nuclei cause the increase in the linewidth by 1.4 mT [41] which is subtracted from ΔB_{pp}. Finally, the τ_1''s in $La_{0.9}Nd_{0.1}F_3$ are evaluated to be $(5.02 \pm 0.3) \times 10^{-13}$, $(1.72 \pm 0.3) \times 10^{-13}$, and $(1.01 \pm 0.2) \times 10^{-13}$ s at 4.2, 77, and 295 K, respectively. The spin–lattice relaxation times of Nd^{3+} ions are dependent on the concentration (x) of diamagnetic La^{3+} ions in mixed crystals $La_xNd_{1-x}F_3$, being longer for bigger concentration. It can be confirmed for τ_1''s at 295 K, because data for the full range of the concentration are available, i.e. 8.87×10^{-15} ($x = 0$), 3.24×10^{-14} ($x = 0.1$) and 1.01×10^{-13} s ($x = 0.9$). The determined τ_1''s at 145 K are as follows: 3.16×10^{-14} ($x = 0$) and 6.30×10^{-14} s ($x = 0.1$).

The spin–lattice relaxation time of Gd^{3+} ions (τ_1) can be determined from the EPR linewidth of Gd^{3+}-doped LaF_3 after subtracting the linewidth equal to 1.4 mT. The estimated τ_1's using Heisenberg's uncertainty rule (assuming $h\Delta\nu = g\mu_B \Delta B_{1/2}$) are equal to 3.7×10^{-9}, 2.8×10^{-9}, and 2.5×10^{-9} s at 4.2, 77, and 295 K, respectively, being longer than τ_1' of host Nd^{3+} ions. It can be assumed that τ_1 of Gd^{3+} ions in $La_{0.9}Nd_{0.1}F_3$ is the same, because the Gd^{3+} spin–phonon interaction constant K_2 does not differ within experimental errors from that in LaF_3 (Gd^{3+}) as shown in Sec. 5. The τ_1 increase by 45% with lowering temperature

from 295 to 4.2 K. This rather small increase is due to weak coupling of Gd^{3+} ions with the lattice, in contrary to strong coupling of Nd^{3+} ions (τ_1' increase by 400% in the same temperature range).

8. Concluding remarks

The small local rotations ($\Delta\varphi = \pm 3.5°$) of the eight fluorine ions (grouped in pairs) surrounding the Gd^{3+} ion, are determined in the Gd^{3+}-doped $La_{0.9}Nd_{0.1}F_3$ when temperature is lowered down to liquid helium. This can induce a slight distortion of the site symmetry of Gd^{3+} ion (C_{2v} to C_2) observed at low temperatures (below 77 K).

The energy of single oscillator has been determined to be 302 cm^{-1} for $La_{0.9}Nd_{0.1}F_3$ and 282 cm^{-1} for LaF_3 using the Einstein model of phonon spectrum. These above average values are somewhat higher than values determined from the Debye model in the long-wavelength limit. The determined Debye temperature 406 K for LaF_3 is close to the realistic value as discussed in Sec. 5.

The main contribution to the observed EPR linewidths of Gd^{3+} in $La_{0.9}Nd_{0.1}F_3$ comes from the strong Nd^{3+} spin–lattice and the Gd^{3+}–Nd^{3+} dipole–dipole interactions. Contribution from the exchange interaction between Gd^{3+} and Nd^{3+} ions plays a secondary role. The Gd^{3+} spin–phonon interaction constant equal to $0.08 \div 0.13$ GHz means that there exist weak interactions of the Gd^{3+} spin with optical phonons at 302 cm^{-1}, due to the zero orbital momentum for Gd^{3+} ($^8S_{7/2}$). It is also concluded that there is more stronger Nd^{3+} spin–phonon interaction, i.e. the Nd^{3+} spin with the optical phonons at 302 cm^{-1}, because the spin–lattice relaxation time (τ_1') of Nd^{3+} ions is four orders of magnitude shorter than that of Gd^{3+} ions (τ_1).

The sum values of magnetoelastic tensor components ($G_{11} + G_{12} + G_{13}$) are calculated for Gd^{3+} ions to be in the range $-3.33 \div -3.04$ GHz for investigated crystals. Further, the values of $\mathcal{R}_D$ in $La_{0.9}Nd_{0.1}F_3$ and LaF_3 crystals show that the rotational contributions to the Gd^{3+} spin-Hamiltonian parameters from phonons are much smaller than those from the strain.

References

[1] E. Auffray, S. Baccaro, T. Beckers, Y. Benhammou, A.N. Belsky, B. Borgia, D. Boutet, R. Chipaux, I. Dafinei, F. de Notaristefani, P. Depasse, C. Dujardin, H. El Mamouni, J.L. Faure, J. Fay, M. Goyot, S.K. Gupta, A. Gurtu, H. Hillemanns, B. Ille, T. Kirn, M. Lebeau, P. Lebrun, P. Lecoq, J.A. Mares, J. P. Martin, V.V. Mikhailin, B. Moine, J. Nelissen, M. Nikl, C. Pedrini, R. Raghavan, P. Sahuc, D. Schmitz, M. Schneegans, J. Schwenke, S. Tavernier, V. Topa, A.N. Vasil'ev, M. Vivargent, J.P. Walder, *Nucl. Instrum. Methods Phys. Res. A* **383**, 367 (1996).

[2] P. Dorenbos, J.T.M. De Haas, C.W.E. Van Eijk, *J. Lumin.* **69**, 229 (1996).

[3] D. Negoy, T. Purohit, *Phys. Status Solidi B* **131**, 329 (1985).

[4] A.A. Kaminskii, H.R. Verdun, *Phys. Status Solidi A* **129**, K119 (1992).

[5] S.K. Misra, P. Mikołajczak, S. Korczak, *J. Chem. Phys.* **74**, 922 (1981).

[6] S.K. Misra, P. Mikołajczak, N.R. Lewis, *Phys. Rev. B* **24**, 3729 (1981).

[7] W. Korczak, M.L. Paradowski, L.E. Misiak, *Phys. Status Solidi B* **165**, 203 (1991).

[8] M.L. Paradowski, W. Korczak, J. Pierre, M. Subotowicz, *Phys. Status Solidi B* **175**, 135 (1993).

[9] M.L. Paradowski, A. Pacyna, A. Bombik, W. Korczak, S.Z. Korczak, *J. Magn. Magn. Mater.* **166**, 231 (1997).

[10] W. Korczak, P. Mikołajczak, *J. Cryst. Growth* **61**, 601 (1983).

[11] M. Mansmann, *Z. Kristallogr.* **122**, 375 (1965).

[12] A. Zalkin, D.H. Templeton, T.E. Hopkins, *Inorg. Chem.* **5**, 1466 (1966).

[13] L. Vegard, *Z. Cryst.* **67**, 239 (1928).

[14] L.E. Misiak, S.K. Misra, P. Mikołajczak, *Phys. Rev. B* **38**, 8673 (1988).

[15] M.L. Paradowski, L.E. Misiak, *Nukleonika* **42**, 543 (1997).

[16] A. Abragam, B. Bleaney, *Electron Paramagnetic Resonance of Transition Ions*, Clarendon, Oxford 1970.

[17] S. K. Misra, *J. Magn. Reson.* **23**, 403 (1976).

[18] L.E. Misiak, P. Mikołajczak, *Acta Phys. Pol. A* **75**, 621 (1989).

[19] F.J. Owens, C.P. Jr. Poole, H.A. Farach, *Magnetic Resonance of Phase Transitions*, Academic Press, New York 1979.

[20] D.J. Newman, W. Urban, *J. Phys. C* **5**, 3101 (1972).

[21] D.J. Newman, W. Urban, *Adv. Phys.* **24**, 793 (1975).

[22] K.W. Blazey, T.L. Estle, E. Holzschuh, W. Odermatt, B.D. Patterson, *Phys. Rev. B* **27**, 15 (1983).

[23] K.A. Müller, W. Berlinger, J. Albers, *Phys. Rev. B* **32**, 5837 (1985).

[24] R. Laiho, M. Lakkisto, T. Levola, *Philos. Mag. A* **47**, 235 (1983).

[25] L.E. Misiak, M. Subotowicz, *Solid State Commun.* **80**, 761 (1991).

[26] E. Liarokapis, E. Anastassakis, G.A. Kourouklis, *Phys. Rev. B* **32**, 8346 (1985).

[27] J. Sytsma, W. Van Schaik, G. Blasse, *J. Phys. Chem. Solids* **52**, 419 (1991).

[28] H. Gerlinger, G. Schaack, *Phys. Rev. B* **33**, 7438 (1986).

[29] G.A. Alers, *Physical Acoustics: Principles and Method*, Vol. 3, Part B, Academic Press, New York 1965.

[30] M.B. Schulz, C.D. Jeffries, *Phys. Rev.* **149**, 270 (1966).

[31] S.B. Oseroff, R. Calvo, *Phys. Rev. B* **5**, 2474 (1972).

[32] N. Guskos, J. Kuriata, T. Rewaj, *Acta Phys. Pol. A* **81**, 659 (1992).

[33] Y.V. Orlowskii, R.J. Reeves, R.C. Powell, T.T. Basiev, K.K. Pukhov, *Phys. Rev. B* **49**, 3821 (1994).

[34] C.A. Bates, H. Szymczak, *Phys. Status Solidi B* **74**, 225 (1976).

[35] C.A. Bates, H. Szymczak, *Z. Phys. B* **28**, 67 (1977).

[36] L.E. Misiak, *Acta Phys. Pol. A* **83**, 195 (1993).

[37] S.K. Misra, U. Orhun, *Phys. Rev. B* **39**, 2856 (1989).

[38] J.H. Van Vleck, *Phys. Rev.* **74**, 1168 (1948).

[39] V.M. Malhotra, J.M. Dixon, H.A. Buckmaster, *Physica B* **101**, 147 (1980).

[40] T. Mitsuma, *J. Phys. Soc. Jpn.* **17**, 128 (1962).

[41] V.K. Sharma, *J. Chem. Phys.* **54**, 496 (1971).